Global-scale hybrid simulation of dayside magnetic reconnection under southward IMF: Structure and evolution of reconnection

B. Tan,[1] Y. Lin,[1] J. D. Perez,[1] and X. Y. Wang[1]

Received 19 April 2010; revised 1 November 2010; accepted 2 December 2010; published 9 February 2011.

[1] Magnetopause reconnection is investigated with our 3-D self-consistent global hybrid simulation model. The magnetic configuration and evolution of Flux Transfer Events (FTEs) and the associated ion density and ion velocity distribution at various locations on the magnetopause are investigated. The results reveal the following. (1) Multiple X lines are formed during the magnetopause reconnection, which lead to both FTEs and quasi-steady-type reconnection under a steady solar wind condition. The resulting bipolar signature of local normal magnetic field of FTEs is consistent with satellite observations. (2) A greater-than-20% plasma temperature rise is seen at the center of a FTE, compared to that of the upstream plasma in the magnetosheath. The temperature enhancement is mainly in the direction parallel to the magnetic field because of the mixing of ion beams. (3) Flux ropes that lead to FTEs form between X lines of finite lengths and evolve relatively independently. The ion density is enhanced within FTE flux ropes because of the trapped particles, leading to a filamentary global density. (4) Different from the previous understanding based on the asymmetric density across the magnetopause, a quadrupole magnetic field signature associated with the Hall effects is found to be present around FTEs. (5) A combination of patchy reconnection and multiple X line reconnection leads to the formation of reconnected field lines from the magnetosphere to IMF, as well as the closed field lines from the magnetosphere to the magnetosphere in the magnetopause boundary layer.

Citation: Tan, B., Y. Lin, J. D. Perez, and X. Y. Wang (2011), Global-scale hybrid simulation of dayside magnetic reconnection under southward IMF: Structure and evolution of reconnection, *J. Geophys. Res.*, *116*, A02206, doi:10.1029/2010JA015580.

1. Introduction

[2] As a concept proposed by *Dungey* [1961], magnetic reconnection is believed to play an important role in geomagnetic and magnetospheric plasma processes. Without magnetic reconnection, the magnetosphere of the Earth is a relatively "isolated" space from the solar wind. With the magnetospheric field lines opened up by the reconnection process, solar wind plasma is able to penetrate through the magnetopause; momentum and energy can also be transferred from the solar wind and interplanetary magnetic field (IMF) into the magnetosphere as the connectivity of the magnetic field lines changes.

[3] One of the important questions about magnetic reconnection is the magnetic configuration of connectivity associated with it, that is, whether the reconnection occurs through a single X line or multiple X lines [*Winglee et al.*, 2008]. According to the time scales of the in situ observation results, magnetic reconnection events fall into two categories: (1) quasi-stationary magnetic reconnection and (2) transient magnetic reconnection. A quasi-stationary magnetic reconnection might have a time scale of hours [*Gosling et al.*, 1982], which is dominated by a single X line. The transient counterpart usually has a quasi-period around 8 min [*Rijnbeek et al.*, 1984]. Flux transfer events (FTEs), which are widely considered to be associated with transient magnetic reconnection nearby [e.g., *Hasegawa et al.*, 2006; *Kuznetsova et al.*, 2009], were first discovered by *Russell and Elphic* [1978]. Initially, FTEs were thought to be flux tubes that are the products of single-X-line, patchy reconnection [*Russell and Elphic*, 1978]. Because of complicated geometries and the multiscale nature of reconnection, numerical simulations have been utilized to investigate the reconnection physics. *Lee and Fu* [1985] suggested that FTEs are multiple-X-line flux ropes with helical internal structures, in which a magnetic field line is reconnected at two or more reconnection sites. Alternative models were also proposed to account for the formation of FTEs. For example, *Scholer* [1988] suggested that the variation of reconnection rate could give rise to loop-like field lines based on the single-X-line reconnection.

[4] Since local simulation models have strong dependence on the boundary conditions, three-dimensional (3-D) global simulations using modern computers have become a powerful tool to study the reconnection and the associated structure

[1]Physics Department, Auburn University, Auburn, Alabama, USA.

0148-0227/11/2010JA015580

of the dayside magnetopause. The latest work includes global magnetohydrodynamic (MHD) simulations by *Fedder et al.* [2002], *Raeder* [2006], *Dorelli and Bhattacharjee* [2009], *Kuznetsova et al.* [2009], and *Winglee et al.* [2008]. *Dorelli and Bhattacharjee* [2009] point out that it is likely that the resistive MHD Ohm's law may fail to capture much of the physics relevant to the FTE generation when the model assumption is no longer valid under certain circumstances.

[5] The challenge to the understanding of FTEs in the magnetopause reconnection is that they are of 3-D nature, embedded in a multiscale solar wind-magnetosphere global system, in which the ion physics is very important. Inclusion of plasma kinetic physics is necessary for the modeling of the generation and evolution of magnetopause reconnection as well as the understanding of their internal structure.

[6] For the first time, here we present a numerical simulation of dayside reconnection using a 3-D global-scale hybrid model, in which fully-kinetic ion physics is solved in a self-consistent electromagnetic field [*Lin and Wang*, 2005]. The reconnection events are identified by the connectivity change of magnetic field lines and supported by the presence of reconnection jets away from the reconnection sites. Both multiple X line and single X line type structures are examined, where the term "X lines" is defined in the context of local 3-D field configuration [e.g., *Priest and Forbes*, 2000]. The detailed definition will be given in section 3.2. Note that our definition of X line is different from the one used by *Dorelli and Bhattacharjee* [2009], which defines the X line as a separator line, the intersection of two separatrix surfaces that separate topologically distinct field lines of four different global regions of magnetic open field lines, field lines between solar wind and south pole, field lines between solar wind and north pole, and closed field lines. Based on a global MHD simulation, *Dorelli and Bhattacharjee* [2009] have found that the instability associated with FTEs is triggered by a movement of the flow stagnation point away from the magnetic separator, which modifies the subsolar stagnation point flow.

[7] In this paper, two cases with a purely southward IMF are investigated. In the presence of a strong southward IMF, the Earth's dipole field is antiparallel to the IMF around the equatorial plane, leading to the occurrence of magnetic reconnection at the low-latitude magnetopause. Statistical studies show that majority of FTEs are observed during a southward IMF [*Rijnbeek et al.*, 1984; *Sibeck and Lin*, 2010]. In section 2, we describe the simulation model; the results are presented in the section 3, followed by a summary in section 4.

2. Simulation Model

[8] We adopt the global hybrid simulation scheme described by *Swift* [1996] and implemented by *Lin and Wang* [2005] for 3-D simulations of the dayside magnetosphere. Note that our simulation addresses the reconnection processes within the dayside convection time scale and not for the entire global magnetosphere. Except for the inner magnetosphere of $r < 7R_E$, the ions (protons) are fully kinetic particles, and the equation in the simulation units for ion motion, is given by

$$\frac{d\mathbf{v_i}}{dt} = \mathbf{E} + \mathbf{v_i} \times \mathbf{B} - \nu(\mathbf{V_i} - \mathbf{V_e}), \tag{1}$$

where $\mathbf{v_i}$ is the ion particle velocity, $\mathbf{E}$ is the electric field in units of ion acceleration, $\mathbf{B}$ is the magnetic field in units of the ion gyrofrequency [*Swift*, 1996] while $\mathbf{V_i}$ and $\mathbf{V_e}$ are the bulk flow velocities of the ions and electrons, respectively. A small current-dependent collision frequency, $\nu \simeq 0.01\Omega J/J_0$, is imposed in order to trigger magnetic reconnection in the simulation, where Ω is the local ion gyrofrequency and $J_0 = B_0/\mu_0\lambda_0$ (here λ_0 is the ion inertial length of the solar wind). A fluid approximation is used to model the inner magnetosphere of $r < 7R_E$, given that the fluid plasma in this region is not expected to affect the kinetics in the region of the magnetopause.

[9] The electrons are treated as a massless fluid, and quasi charge neutrality is assumed in the calculation. The electric field is determined by the electron momentum equation

$$\mathbf{E} = -\mathbf{V_e} \times \mathbf{B} - \nu(\mathbf{V_e} - \mathbf{V_i}) - \nabla \mathbf{P_e}/\mathbf{N}, \tag{2}$$

where $\mathbf{V_e}$ is the electron bulk flow velocity, P_e is the thermal pressure of electrons and N is the electron number density. The magnetic field is updated by Faraday's law,

$$\frac{\partial \mathbf{B}}{\partial t} = -\nabla \times \mathbf{E}. \tag{3}$$

[10] In the presentation below, the magnetic field B is scaled by the IMF B_0; the ion number density N by the solar wind density N_0; the time t by the inverse of the solar wind ion gyrofrequency (Ω_0^{-1}); the flow velocity V by the solar wind Alfvén speed V_{A0}; the temperature by V_{A0}^2; the length in units of the Earth's radius R_E.

[11] In order to accommodate to the available computing resources, a larger-than-reality ion inertial length $\lambda_0 = 0.1R_E$ of the solar wind is chosen in the simulation. Note that $V_{A0} = \lambda_0\Omega_0$. In an effort to examine the effects of various values of λ_0, we have also run a case with $\lambda_0 = 0.05R_E$, although still about 3 times larger than that in reality. The resulting structures of the magnetopause reconnection are qualitatively the same as that shown in this paper.

[12] Spherical coordinates are used in the simulation. The polar angle θ is measured from the positive GSM z axis, and the azimuthal (longitudinal) angle ϕ from the negative GSM y axis. The simulation domain contains the system of the bow shock, magnetosheath, and magnetosphere in the dayside region with GSM $x > 0$ and a geocentric distance $4 \le r \le 24.5$. The Earth is located at the origin $(x, y, z) = (0, 0, 0)$. Outflow boundary conditions are utilized at $x = 0$, while inflow boundary conditions of the solar wind are applied at $r = 24.5$. The inner boundary at $r = 4$ is perfectly conducting.

[13] Initially, a geomagnetic dipole field plus a mirror dipole is assumed in $r < 10R_E$ [*Lin and Wang*, 2005], and a uniform solar wind with the IMF B_0 of $B_{x0} = 0$, $B_{y0} = 0$ and $B_{z0} = -1$ is imposed for $r > 10R_E$. The mirror dipole in the initial setup is to speed up the formation of the bow shock and magnetopause. The bow shock, magnetosphere and magnetosheath are formed by interaction between the solar wind and the dipole field.

[14] We choose a uniform solar wind with $\beta_i = \beta_e = 0.5$ and an Alfvén Mach number $M_A = 5$. The solar wind flows into the system along the $-x$ direction with an isotropic drifting-Maxwellian distribution. The ion number density in the solar wind is set to be $N_0 = 11{,}000R_E^{-3}$ for macro particles in this

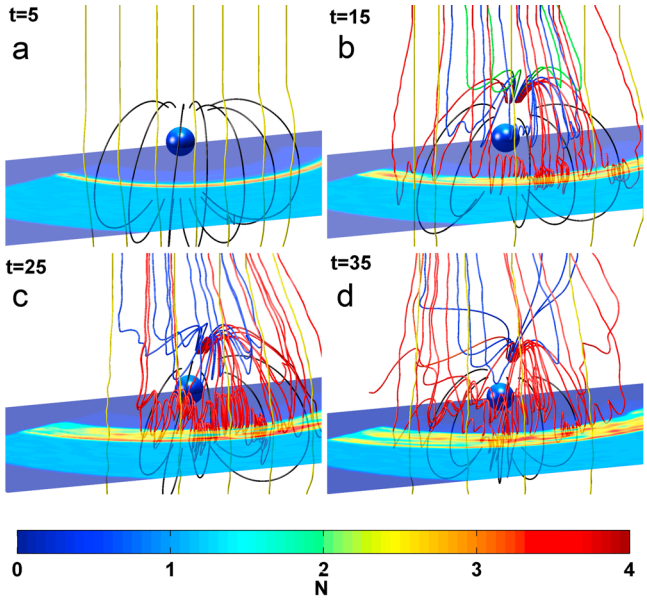

Figure 1. Magnetic field line configuration in a global view obtained in case 1 at (a) $t = 5$, (b) $t = 15$, (c) $t = 25$, and (d) $t = 35$. The closed dipole field lines are in black. Yellow lines are open field lines before magnetic reconnection. Field lines in other colors are reconnected field lines between the IMF and dipole field in different regions. Contours in the equatorial plane show the ion density.

kinetic simulation, and a total of $\sim 4 \times 10^8$ particles are used in a run. For a typical ion gyrofrequency of 0.1 s^{-1}, the corresponding IMF is $\simeq$10 nT.

[15] Nonuniform grid spacing Δr is used to produce a higher resolution near the magnetopause, where $\Delta r \simeq 0.09 R_E$. A total grid of 160 × 104 × 130 is used. The time step to advance the positions of ions is 0.05.

[16] Two cases are presented in the following. In case 1, the dipole axis is tilted sunward by 15°, so that the northern cusp region is well within the simulation domain. Case 2 is similar to case 1, except that the dipole tilt angle is equal to zero.

3. Simulation Results

3.1. Magnetic Field Line Configuration Under Southward IMF

[17] We first present results from case 1, with a 15° dipole tilt angle. As the solar wind ions convect earthward carrying the IMF, the bow shock, magnetosheath, and magnetopause form gradually in a self-consistent manner. Most magnetic reconnection events originate in the equatorial region, which are related to X lines of nearly antiparallel magnetic field reconnection. Flux ropes are generated above and below the equator and reconnected magnetic field lines are approximately symmetric about the noon meridian plane.

[18] Figure 1 shows the magnetic field line configuration obtained from case 1 in a global view, emphasizing field lines in the northern hemisphere at $t = 5$, 15, 25, and 35. The blue sphere at the origin represents the Earth. The contours in the equatorial plane show the ion density. Outward from the Earth, the boundary region with a sharp ion density increase is the magnetopause, at a standoff distance of $r \simeq 9.5 \sim 10$. The bow shock is the boundary region with a sharp density decrease. The black lines are the closed field lines of the geomagnetic dipole field. The yellow lines are open field lines of the shocked IMF before magnetic reconnection. Field lines in other colors are reconnected field lines with one end connecting to IMF and the other end to the magnetosphere, where the colors are used to distinguish different regions of magnetic reconnection as in the description below.

[19] Figure 1a shows the magnetic configuration of the initial phase at $t = 5$, or $t \simeq 25\Omega^{-1}$ with Ω^{-1} being the local ion gyrofrequency. There appears to be no significant evidence of magnetic reconnection at this time.

[20] At $t = 15$ (Figure 1b), looped flux ropes (FTEs), form in between two neighboring X lines, while the X lines of finite length lie in the dawn-dusk direction. The axial extent of the flux ropes is limited as seen in the plot. Around the equator, there are both looped flux ropes and adjacent single X line magnetic reconnection shown by the red field lines. FTEs are found to be localized looped flux ropes corresponding to multiple X line reconnection (MXR) [*Raeder*, 2006; *Hasegawa et al.*, 2006] with helical internal structures, which generate signatures consistent with in situ observations. The bipolar FTE signature of B_n, the local normal component of magnetic field, will be discussed below. A Walén test will also be performed for the single X line reconnection to investigate the presence of relevant MHD discontinuities, using the data from case 2. The blue field lines in the mid-latitudes show another layer of looped flux ropes (FTEs), while the green field lines in the northern high latitudes show the occurrence of a single X-line-type reconnection with no obvious looped field lines.

[21] At $t = 25$ (Figure 1c), or $t \simeq 125\Omega^{-1}$, the looped flux ropes illustrated by the red field lines of $t = 15$ have moved poleward with a noticeable expansion of their azimuthal size. The blue FTEs at $t = 15$ have also propagated toward the cusp and tailward, and meanwhile toward dawn/dusk side.

[22] At $t = 35$ (Figure 1d), part of the red flux ropes around the equator at $t = 15$ have moved to the middle latitudes, so have segments of X lines adjacent to the FTEs. The blue FTEs in the middle latitudes at $t = 15$ also continue moving tailward and poleward, and part of them have disintegrated during the interaction with the cusp while the rest have convected past the pole.

[23] In our simulation, the magnetopause reconnection is found to generate not only the reconnected field lines connecting the IMF to the dipole field, but also other topologies due to 3-D effects, including both purely closed reconnected field lines as well as purely open reconnected field lines. The color plots in Figure 2a show four field lines of case 1 at $t = 55$, in which the flux ropes are mainly located at $x \simeq 9.5$–10, $y \simeq -0.6$–1.8 and $z \simeq -0.5$–1. In addition to the blue and black field lines that are between the magnetosphere and the magnetosheath, there also exist the green closed field lines that are connected from the magnetospheric field to the magnetospheric field, threading from the northern cusp to the southern cusp, as well as the red open field line from the magnetosheath to the magnetosheath. The rectangular contour slice shows ion density at $z = 0.5$ around the reconnection site. Note that the sliver of green density on the slice is adjacent and on the sunward side of the flux ropes.

[24] The green and red field lines in Figure 2 are associated with the FTE flux ropes, and thus are different from the

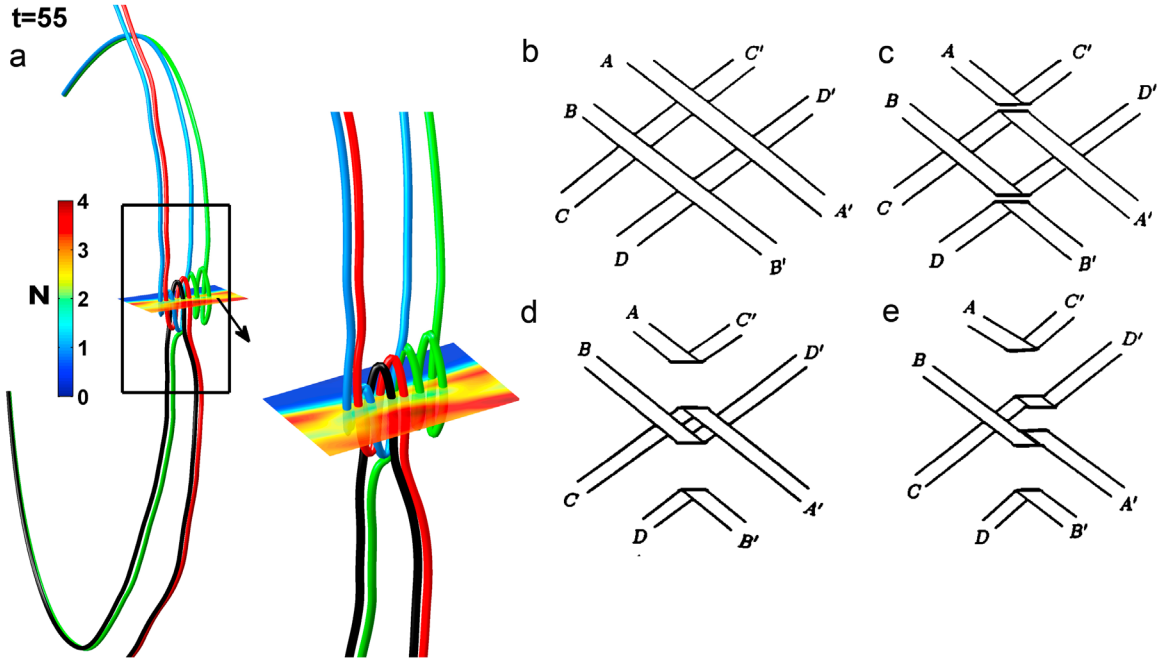

Figure 2. (a) Four field lines of different topologies in case 1 at $t = 55$. (b-e) Illustrations of how the patchy reconnection and multiple reconnection can explain the coexistence of the four field lines in Figure 2a [*Lee et al.*, 1993].

unperturbed closed geomagnetic field lines and open solar wind field lines. A previous 3-D MHD simulation of *Lee et al.* [1993] shows that because of the nonuniformity along the plane of the current sheet, four possible topologies of FTE field lines can be generated. They are the field lines connected (1) from IMF to the Earth's dipole field (field lines between solar wind and north pole), (2) from the Earth's dipole field to the Earth's dipole field, (3) from the Earth's dipole field to IMF (field lines between solar wind and south pole), and (4) from IMF to IMF. Figures 2b–2e [*Lee et al.*, 1993] can be used to illustrate how the patchy, multiple reconnection events can explain the coexistence of the four types of field lines obtained from our 3-D simulation as shown in the color plots of Figure 2a. The patchy reconnection indicates that the size of the reconnection region has a fairly limited extent in space [*Kan*, 1988; *Pinnock et al.*, 1995]. At the initial stage (Figure 2b), flux tubes AA′ and BB′ are two bundles of magnetosheath fields and CC′ and DD′ are of magnetospheric fields. At the second stage (Figure 2c), reconnection takes place at two patches. At the third stage (Figure 2d), the reconnected flux tubes BD′ and CA′ move toward each other so that at the fourth stage (Figure 2e) a re-reconnection has occurred, leading to the formation of closed flux tube CD′. Flux tubes CD′ and BA′ correspond to the green (closed) and red (open) field lines in the color plots of Figure 2a. Since flux ropes form between multiple X lines, a position shift of neighboring X lines relevant to flux ropes can also play a critical role in determining the connectivity of field line [*Lee et al.*, 1993].

[25] The existence of reconnected field lines from the magnetosphere to the magnetosphere or from IMF to the IMF, in addition to the opened magnetospheric field lines and the unperturbed magnetosheath field lines, has also been suggested by *Lui et al.* [2008] and *Kuznetsova et al.* [2009]. In our simulation, localized flux ropes at low latitudes with dominant purely closed field lines do not occur often and cannot survive more than $20\Omega_0^{-1}$. Further investigation is needed to address how long their life time is for more general cases with a finite IMF B_y component.

3.2. Structure and Evolution of FTEs

[26] The structure and evolution of FTEs are illustrated in Figure 3 around the dayside magnetopause. Here we give our definition of the reconnection X line before the discussion on physical quantities associated with 3-D reconnection. We adopt a procedure like the one described by *Priest and Forbes* [2000], which defines reconnection in a general way.

[27] We seek a set of singular lines, near which the magnetic field has an X type configuration. Figures 3a and 3b illustrate how a singular line, or in another word, "X line," is defined, which is the intersection of two surfaces that separate distinct field lines of four different local regions (earthward side of the magnetopause current sheet, sunward side of the current sheet, from the sunward side to the earthward side, and from the earthward side to the sunward side following the magnetic field direction). The black tubes are field lines traced in the 3-D space. The X type configuration is determined by mapping the 3-D field lines into an x-z reference plane. An X point of the X line that separates local areas of four different magnetic connectivity types is found, shown as a blue dot. By connecting the X points in a series of such planes, an X line segment naturally forms. Other supporting evidence of the X line, such as the existence of opposite flow jets and the quadrupole magnetic field structure in the guide field, is given below. The FTEs to be discussed in this paper are of an O line that requires two X lines.

[28] As shown in Figure 3a, there are two X line segments as blue dots at $t = 15$. There are also two X lines at $t = 65$. But

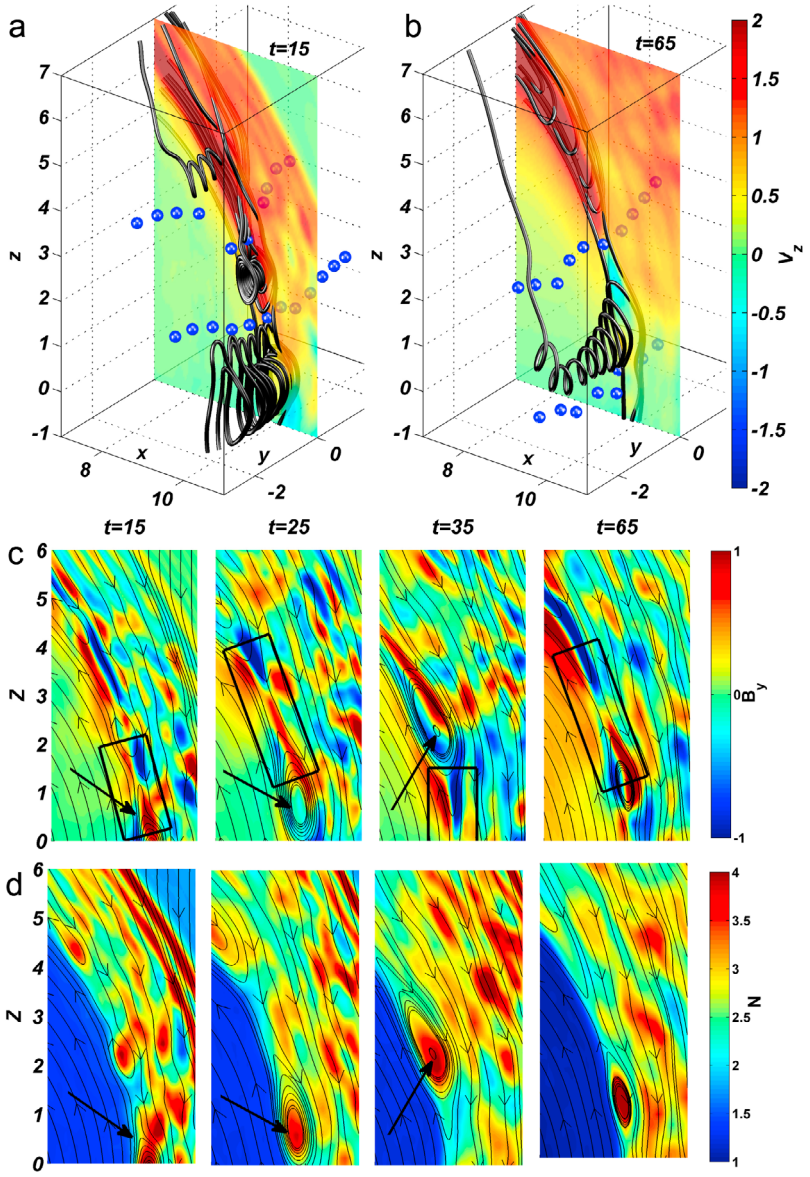

Figure 3. (a and b) Three-dimensional plots illustrate how X line is defined, with V_z contours in the noon meridian plane. Two dimensional intensity plots of (c) B_y, (d) ion density, (e) total magnetic field, (f) parallel temperature, and (g) perpendicular temperature are also in the noon-midnight meridional plane, zoomed around the dayside magnetopause at t = 15, t = 25, t = 35, and t = 65 (from left to right).

the previous two at t = 15 are not seen at t = 65 as they have moved northward. The northern X line segment at t = 65 was below the plane of z = −1 at t = 15 before it moves to its present location in this case with a tilted dipole axis.

[29] In order to illustrate the presence of reconnection jets from the X lines, the contours in Figures 3a and 3b show V_z, the z component of ion bulk flow velocity in the noon-midnight meridional plane obtained from case 1. Our definition of the 3-D magnetic reconnection is consistent with observations that plasma jets are moving away from X lines due to reconnection. At t = 65, two opposite jets with V_z of opposite sign occur inside the FTE flux ropes between the two X lines. The V_z of magnetosheath plasmas near FTEs increases as the latitude increases. Although two opposite jets are expected from an X line, the southward jet at t = 15 appears missing, because of the nonzero northward background V_z of the ambient magnetosheath plasmas. Meanwhile, strengths of the two opposite jets from two adjacent X lines inside one FTE are not necessarily equal to each other. As in the case at t = 15 shown in Figure 3a, one direction of ion acceleration is dominant inside the FTE between the two X lines.

[30] The intensity plots in Figure 3 show B_y (Figure 3c), ion density N (Figure 3d), magnetic field strength B (Figure 3e), parallel ion temperature $T_{||}$ (Figure 3f), and perpendicular ion temperature $T_{\perp}$ (Figure 3g) in the noon-midnight meridional plane at t = 15, 25, 35, and 65. The black lines superposed on the contours are two dimensional (2-D) field lines projected

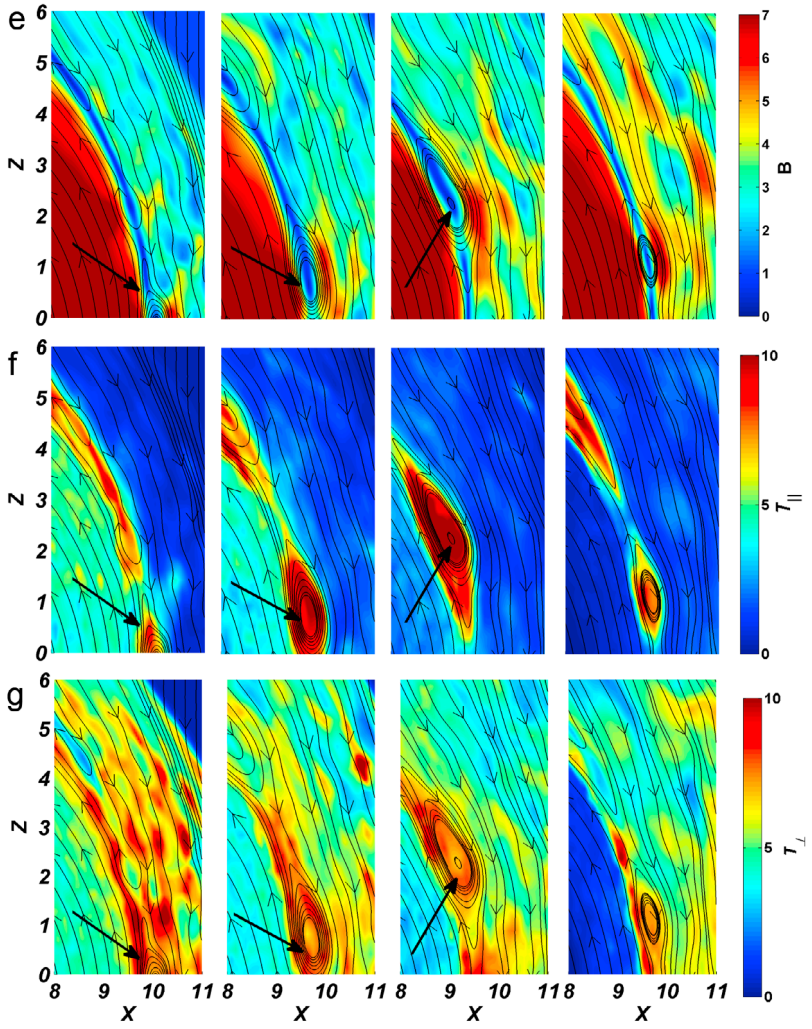

Figure 3. (continued)

onto the noon meridian plane. Note that the density of 2-D field lines shown here does not represent the magnetic field strength. The locations of FTEs can be identified from the magnetic islands traced by the field lines in the contour plots. The center of a highlighted FTE island is marked with arrows in the plots from $t = 15$ to $t = 35$.

[31] The FTE marked in Figure 3 forms around $t = 15$ at the subsolar region and moves poleward as time proceeds. The FTE speeds up as it moves away from the equator. At $t = 65$, another FTE forms near the subsolar region, which reflects the quasiperiodic generation of FTEs. Between $t = 35$ and $t = 65$, there is a relative quiescent period, and magnetic reconnection remains single X-line-like in the region.

[32] Perturbations in B_y are obtained in the vicinity of X lines, as indicated by the black rectangles in Figure 3. Because the initial B_y in the solar wind is set to be zero, the intensity of B_y in the plot can be viewed as a perturbation. The B_y pattern is consistent with the Hall effects due to the ion kinetic effects [*Sonnerup*, 1979; *Terasawa*, 1983; *Pritchett*, 2001; *Shay et al.*, 2001]. In a simple 2-D reconnection model, plasma flows into the vicinity of an X line. Electrons are frozen-in to the field lines and ions lag behind due to their larger inertia, which produces a net current and a corresponding B_y perturbation. This leads to a negative B_y above and a positive B_y below the X line on the magnetosheath side, with a negative B_y below and a positive B_y above the X line on the magnetospheric side. For the dayside magnetopause, it is expected that the polarity on the magnetosheath side dominates the Hall pattern due to the much larger density on the magnetosheath side, which is different from the quadrupole structure of B_y for a nearly symmetric current sheet [*Karimabadi et al.*, 1999; *Pritchett*, 2001; *Birn et al.*, 2008].

[33] In contrast to a dominant polarity on the magnetosheath side, B_y perturbations with near equal strength are seen in the multiple X line reconnection at $t = 25$, 35 and 65 in our simulation, as shown in Figure 3. The quadrupole B_y perturbations are within a boundary layer, of which the sunward thickness is $\sim 0.5R_E - 1.0R_E$. The plasma density level in the boundary layer adjacent to the magnetosphere is about 1.0, comparable to 2.0, in the ambient magnetosheath. The local plasma density adjacent to the magnetosphere may be enhanced by the trapped ions around the nearby O line of an

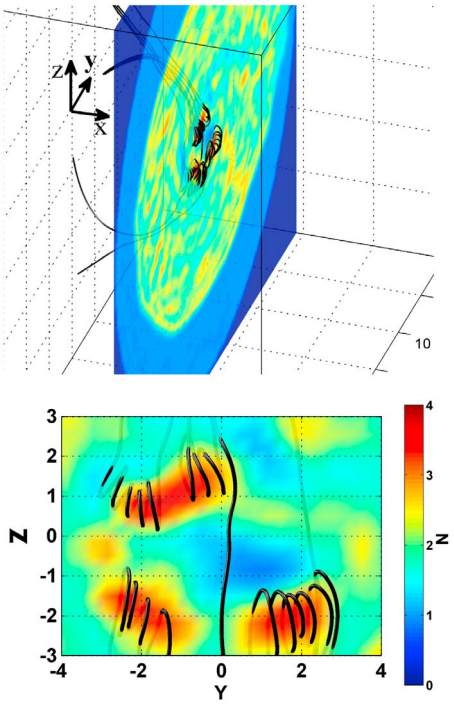

Figure 4. Ion density filaments inside FTEs of case 1. (top) Ion density contours at $x = 9.5$ and $t = 80$, superposed onto a field-line plot; (bottom) a close-up of the same plane.

FTE. The presence of near quadrupole B_y may be due to the thick boundary layer around the FTEs.

[34] Figure 3d reveals that the FTEs are associated with ion density enhancements at the core. Note that the low-density region at $t = 15$, $x = 10$–11 and $z = 5$–6 are in the solar wind. Corresponding to the density enhancement, the magnetic field strength is found to dip in the core of the FTE as seen in Figure 3e. Such results are consistent with the 2-D hybrid simulation results of *Omidi and Sibeck* [2007] for a similar case of a purely southward IMF, in which the reconnection is mainly of antiparallel field type. It has been suggested [e.g., *Hasegawa et al.*, 2006; *Scholer et al.*, 2003] that whether an FTE possesses a strong core field may be associated with whether the reconnection is an antiparallel or component merging.

[35] In Figure 4 (top), ion density contours at $x = 9.5$ at $t = 80$ are shown as well as field lines, while a close-up plot around three FTEs at the magnetopause is shown in Figure 4 (bottom). The flux ropes are seen to wrap around a filament of relatively higher ion density. The peak density is about 2 times that of the ambient plasma inside the boundary layer. Our results indicate that the density at the FTE core may be larger than that near the edge, and that the spatial profile of the density along a path through the core may be very different from that through the edge.

[36] Ion heating is found in the FTEs, as shown in Figures 3f and 3g. Stronger enhancement in the parallel ion temperature $T_{\|}$ is seen inside FTEs, while the perpendicular temperature $T_{\perp}$ shows a mild increase compared with that in the ambient magnetosheath. The enhancement of $T_{\|}/T_{\perp}$ in magnetic reconnection has also been reported in satellite observations [*Klumpar et al.*, 1990] and numerical simulations [*Birn and Hesse*, 2001]. Note that the fading of the ion temperature in the closed field line region between $t = 15$ and $t = 65$ is due to the loss of ion particles in the magnetosphere because the returned ions from the magnetotail are not included in the simulation model. Only the transmitted ions from the magnetosheath are emphasized in the simulated magnetopause reconnection.

3.3. Bipolar Magnetic Field Signature and Ion Velocity Distributions in FTEs

[37] Bipolar signature of the normal component of magnetic field, B_n, has been considered a typical signature of the observed FTEs [e.g., *Russell and Elphic*, 1978; *Dorelli and Bhattacharjee*, 2009]. Viewed in the local normal coordinates, satellites traveling through an FTE along the magnetopause usually observe a transient magnetic field structure in which B_n changes either from positive to negative or from negative to positive.

[38] The flux ropes obtained in our simulation indeed produce the bipolar signature similar to satellite observations. Figure 5d shows the spatial variation of the magnetic field and ion density along a virtual satellite path through the magnetospheric edge of an FTE at $t = 40$ in the simulation of case 1. In the contour plots of Figure 5, the path is from point $P1$ to point $P2$ along the magnetopause, illustrated by the thick black line. The contours are of N, B_y and V_z in the noon meridian plane, with 2-D black field lines superposed on.

[39] The top three panels in Figure 5d show the spatial variations of B_n, B_l, and B_m components of magnetic field, where the local normal direction $\hat{\mathbf{n}}$ of the *lmn* local coordinate system is determined by the minimum variance method [*Sonnerup and Cahill*, 1967]. In this coordinate system, three directions $\hat{\mathbf{l}}$, $\hat{\mathbf{m}}$ and $\hat{\mathbf{n}}$ complete a right-handed orthogonal system with $\hat{\mathbf{l}}$ defined as $(\hat{\mathbf{z}} - \hat{\mathbf{n}}(\hat{\mathbf{n}} \cdot \hat{\mathbf{z}}))/|\hat{\mathbf{z}} - \hat{\mathbf{n}}(\hat{\mathbf{n}} \cdot \hat{\mathbf{z}})|$ and $\hat{\mathbf{m}}$ as the vector product $\hat{\mathbf{n}} \times \hat{\mathbf{l}}$.

[40] The local normal direction $\hat{\mathbf{n}}$ is found to be (0.8259, 0.0139, 0.5636) and $\hat{\mathbf{m}}$ is nearly $-\hat{\mathbf{y}}$ in the GSM system. As shown in the top panel of Figure 5d, B_n changes from positive near $P1$ to negative as the virtual satellite "flies" toward $P2$, consistent with the typical bipolar magnetic field signature of FTE. The B_l component remains a positive magnetospheric value during the crossing. The magnitude of B_m is approximately equal to $-B_y$. The two bipolar enhancements of B_m are due to two parts of the adjacent Hall field perturbations from two X lines as illustrated in the contours of B_y. Near the center of the FTE, the ion density goes up as the virtual satellite cuts through the density filament inside the flux ropes as shown in the contours of N. The bottom panel of Figure 5d shows the field strength B, which exhibits a pattern that is not of a simple antiphase relationship with ion density.

[41] To investigate the properties of ion particles around FTEs, we "probe" the ion velocity distributions (Figure 6) at the specific FTE highlighted with white dots in Figure 5. Figure 6 plots the parallel velocities (relative to the local magnetic field) $v_{i\|}$ of ion particles versus one of the two perpendicular ion velocities, $v_{i\perp 1}$. Here the perpendicular direction $\hat{\mathbf{e}}_{\perp \mathbf{1}}$ is chosen to be in the direction of $\mathbf{B} \times \hat{\mathbf{y}}$. Figure 6 shows the distributions at four chosen locations centered at $D1$ (Figure 6, top left), $D2$ (Figure 6, top right), $D3$ (Figure 6, bottom left), and $D4$ (Figure 6, bottom right), which are marked in the contours of Figure 5.

[42] Figure 6 (top left) corresponds to location $D1$ centered at $(x, y, z) = (8.08, 0, 2.62)$. Among the four locations, $D1$ is

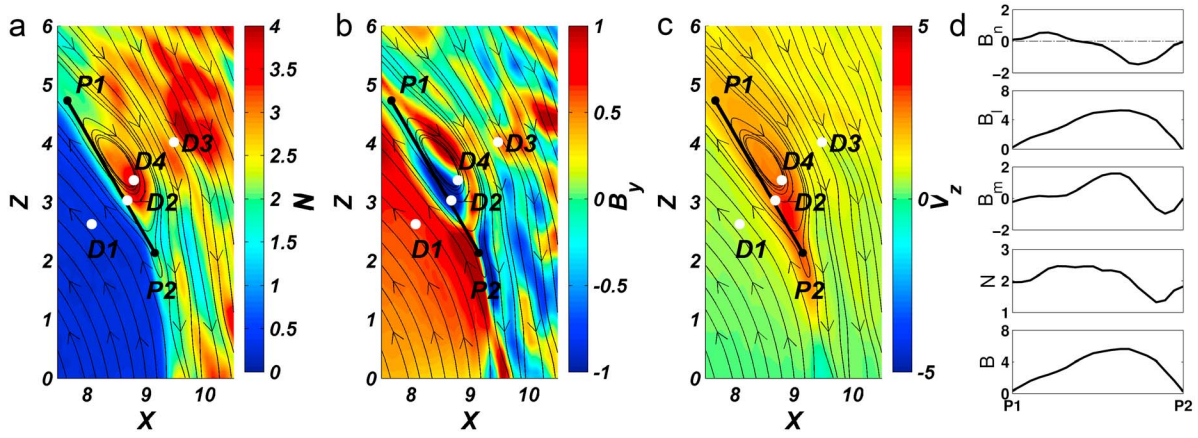

Figure 5. (a-c) Ion density, B_y and V_z in the noon meridian plane around an FTE in the dayside magnetopause in case 1. The thin black lines are projected field lines. The thick black line from point *P*1 to point *P*2 is a virtual satellite pass. *D*1, *D*2, *D*4 and *D*3 are four locations in the magnetopause, inside the FTE, near the center of the FTE, and in the magnetosheath, respectively. (d) Variations of magnetic field and ion density along the virtual satellite pass at $t = 40$.

the closest to the magnetosphere but still on open field lines. The velocity distribution features a tenuous ion population, and the majority of ions possess near zero bulk velocity. Figure 6 (bottom left) corresponds to location *D*3 centered at $(x, y, z) = (9.48, 0, 4.02)$ in the magnetosheath outside the FTE. This dense ion population convects northward with the bulk $V_{i||} < 0$, opposite to the southward IMF.

[43] Figure 6 (top right) corresponds to location *D*2, centered at $(x, y, z) = (8.69, 0, 3.03)$, which is well inside the flux ropes. Figure 6 (bottom right) corresponds to location *D*4, centered at $(x, y, z) = (8.83, 0, 3.27)$, which is near the center of the flux ropes. Mixtures of multiple ion beams transmitted from the magnetosheath are seen in the $v_{i||} - v_{i\perp 1}$ plane. The presence of multiple ion beams in FTEs has also been reported from satellite observations [e.g., *Hasegawa et al.*, 2006]. The velocity distributions at *D*2, *D*4 feature the highest ion temperatures among the selected locations, with $T_{||} > T_{\perp}$ as indicated by the larger extent of the contours in $v_{i||}$ than that in the perpendicular velocity space of $v_{i\perp 1}$ and $v_{i\perp 2}$ (not shown). The majority of ions possess a large positive velocity $v_{i||}$ at *D*2 while the majority of ions at *D*4 possess a large negative velocity $v_{i\perp 1}$. Positive $v_{i||}$ at *D*2 and negative $v_{i\perp 1}$ at *D*4 both indicate that these ions are accelerated northward away from the X line south to the FTE that the four locations are associated with. Several other locations to the north of *D*2 and *D*3 and inside the FTE were probed and the results show that ions are also accelerated northward away, which is consistent with the positive V_z shown in the contour plot.

3.4. Walén Test of Rotational Discontinuity

[44] To evaluate the influence of the tilt angle of the Earth's dipole field, we have run case 2 with the same parameters except that the tilt angle is chosen to be zero. It is found that under the new condition, X lines also form and move poleward. Although the time scale of the reconnection in case 2 is of the same order as in case 1, the average time of reoccurrence of FTEs from the subsolar region in case 2 is longer. Figure 7a shows an example of case 2 at $t = 100$, where that the magnetic reconnection structure north to the subsolar looped flux ropes is "single-X-line-like." The semitransparent contour plot shows V_z, the z component of the ion flow velocity in the noon meridian plane, illustrating plasma jets away from X lines. As the plot in fact is a 3-D one with a view from dawn to dusk, the black tubes that sometimes pass through the noon meridian plane are true 3-D field lines. While the FTE flux ropes are forming at the subsolar region in the northern hemisphere, a rotational discontinuity is found north to the subsolar looped flux ropes, associated with a single X line. Note that in case 1 with a dipole tilt of 15°, the magnetopause is dominated by FTEs as also found in the 3-D global MHD simulation of *Raeder* [2006]. No clear rotational discontinuities are found in case 1.

[45] Both theoretical models [e.g., *Lin and Lee*, 1994], and observations [*Phan et al.*, 1994] show that a large amplitude rotational discontinuity, an intermediate-mode MHD

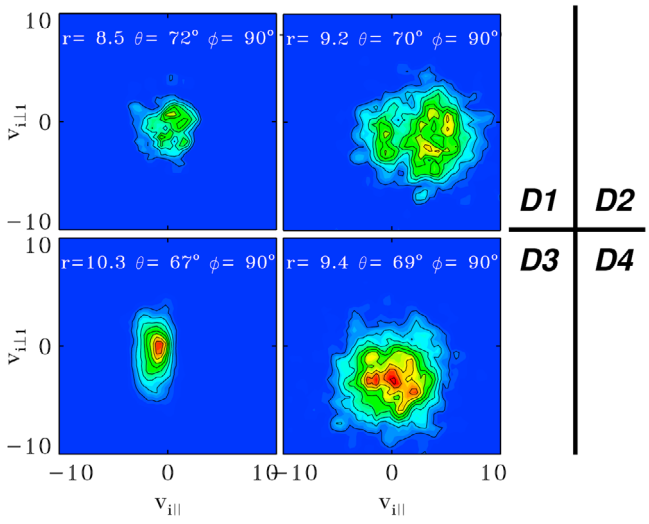

Figure 6. Ion velocity distributions at four chosen locations centered at (top left) *D*1, (top right) *D*2, (bottom left) *D*3, and (bottom right) *D*4, which are marked in the contours of Figure 5.

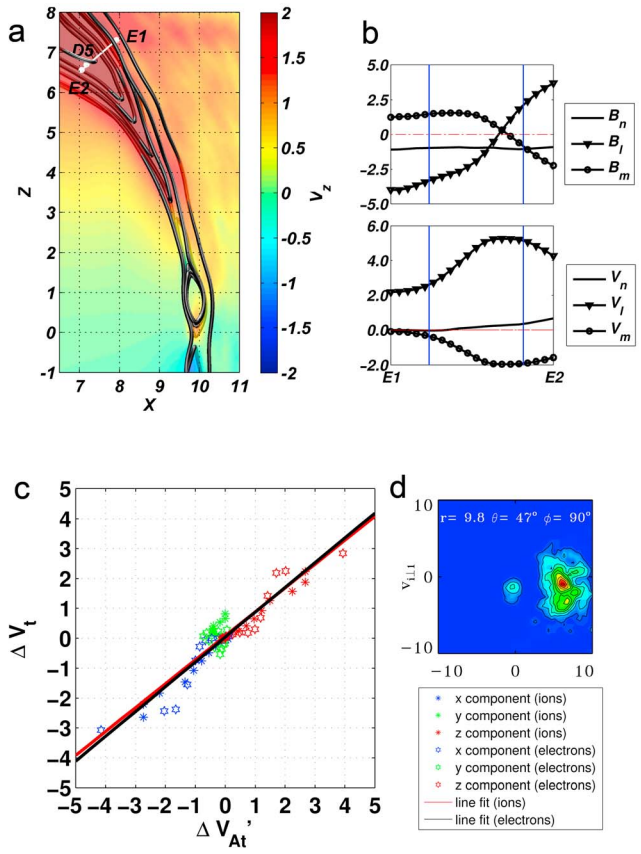

Figure 7. Walén test in case 2 in the northern hemisphere at $t = 100$. (a) Contour plot shows the ion flow velocity V_z in the noon meridian plane, in which $E1$-$E2$ is a line segment in the r direction across a rotational discontinuity. (b) Spatial cuts of field components B_l, B_m, and B_n and ion flow velocities V_l, V_m, and V_n along $E1$-$E2$. (c) The result of Walén test. (d) The ion velocity distribution at location $D5$ between $E1$ and $E2$.

discontinuity, may exist in outflow regions of quasi-steady reconnection at the magnetopause. Here we examine the existence of a rotational discontinuity in the magnetopause boundary layer in our 3-D global-scale hybrid simulation. The Walén relation is applied to identify the rotational discontinuity [*Sonnerup et al.*, 1981], which states that across the rotational discontinuity the tangential plasma flow velocity $\mathbf{V_t}$ changes, as

$$\Delta \mathbf{V_t} = \pm \Delta \mathbf{V_{At}}' = \pm \Delta \mathbf{V_{At}} \left[\mathbf{1} - \left(\beta_{\parallel} - \beta_{\perp}\right)/\mathbf{2}\right]^{\mathbf{1/2}}, \qquad (4)$$

where $\Delta \mathbf{V_t}$ is the change of the tangential flow velocity across the rotational discontinuity and $\Delta \mathbf{V'_{At}}$ is the corresponding change in the tangential Alfvén velocity corrected by a temperature anisotropy factor. The plus (minus) sign is applied to discontinuities with a normal component of the upstream inflow velocity parallel (antiparallel) to the normal component of the magnetic field [*Paschmann et al.*, 1986]. In satellite observations [*Sonnerup et al.*, 1981; *Phan et al.*, 1996] and a previous hybrid simulation [*Lin*, 2001], equation (4) is not exactly satisfied. Instead, Walén ratio $A \equiv |\Delta \mathbf{V_t}|/|(\Delta \mathbf{V_{At}}[\mathbf{1} - (\beta_{\parallel} - \beta_{\perp})/\mathbf{2}]^{1/2})|$ usually ranges from 0.6 to 0.9 for ions, and for electrons the Walén relation can be nearly satisfied [*Scudder et al.*, 1999].

[46] Figure 7 shows an example of Walén test around a single X line reconnection site in case 2 in the northern hemisphere at $t = 100$. The contour plot in Figure 7a shows the V_z component of ion bulk flow velocity in the noon meridian plane, in which the black tubes are 3-D field lines. The magnetic field lines in this plot sometimes cross the noon meridian plane, indicating a nonzero B_y component. $E1$-$E2$ is a line segment in the r direction across the discontinuity to be studied below, while $E1$ is at $(x, y, z) = (7.926, 0, 7.3)$ and $E2$ at $(x, y, z) = (7.059, 0, 6.55)$. Point $D5$ is centered at $(r, \theta, \phi) = (9.8, 47°, 90°)$, also on the path $E1$-$E2$.

[47] A rotational discontinuity is identified along the line cut, of which the local normal direction to the discontinuity, $\hat{\mathbf{n}}$, is determined by the minimum variance method used in section 3.3. The $\hat{\mathbf{l}}$, $\hat{\mathbf{m}}$, $\hat{\mathbf{n}}$ are $(-0.6643, -0.2307, 0.7110)$, $(0.3281, -0.9446, -0.0000)$ and $(0.6716, 0.2333, 0.7032)$ in the GSM system, respectively. Spatial cuts of magnetic field components B_l, B_m, B_n and ion flow components V_l, V_m, V_n along $E1$-$E2$ are shown in Figure 7b. The rotational discontinuity is identified between the two blue vertical lines, across the magnetopause current layer. From $E1$ to $E2$, the normal component of magnetic field remains nearly constant while B_l changes sign. The B_m component, although possessing a sign change too, is dominated by $B_m > 0$, or $B_y < 0$, unlike the quadrupole B_y pattern shown around the case 1 FTEs (Figure 3). Through the sharp kinks of field lines from $E1$ to $E2$ across the magnetopause, the dominant flow component V_l is accelerated from 2.5 in the magnetosheath to 5.3 in the boundary layer, a change of $\simeq$1.46 local Alvén speed, by the field tension force.

[48] Figure 7c shows the result of the Walén test. Throughout the points from $E1$ to the right blue vertical line along the path $E1$-$E2$, $\Delta \mathbf{V_t}$ is obtained by calculating the difference between local $\mathbf{V_t}$ and that at $E1$ on the upstream side of the discontinuity, and the change in Alfv'en velocity $\Delta \mathbf{V'_{At}}$ is calculated similarly [*Paschmann et al.*, 1986]. The blue, green and red hexagrams represent the change of x, y and z component of electron tangential flow velocity versus the change of $\mathbf{V'_{Atx}}$, $\mathbf{V'_{Aty}}$ and $\mathbf{V'_{Atz}}$, respectively. The star-shaped markers show the data for ions. Linear fitting based on the method of least squares is performed to obtain the Walén ratio. The red line is the line fitting result for ions while the black line for electrons. Both slopes are positive because the inflow velocity is parallel to the normal component of magnetic field. The Walén ratio for the electron fluid is about 0.83, shown as the slope of black line, and for ions the number is 0.80, shown as the slope of the red line. This rotational discontinuity is not fully developed as expected for discontinuities not far enough from the X line [*Lin*, 2001]. As a result of our simulation, the perturbation in δB_y is small and the slopes of ions and electrons are not well separated as predicted by the two-fluid theory [*Wu and Lee*, 2000].

[49] Figure 7d shows the ion velocity distributions at location $D5$ in the magnetopause boundary layer. The main population of ions have a positive parallel velocity with a fairly clear cut along a constant minimum $v_{i\parallel}$, and the distributions in the $v_{i\parallel} - v_{i\perp 1}$ plane appears to be a D-shaped distribution [*Cowley*, 1982; *Fuselier et al.*, 1991]. A small fraction (5.2%) of ions, which possess near zero average velocities, are the cold ions initially loaded in the magneto-

sphere. In contrast, no clearly D-shaped velocity distributions of transmitted magnetosheath ions are found at locations around the FTEs in case 1. Along the path *E*1-*E*2, the perpendicular ion temperature $T_\perp$ is larger than the parallel ion temperature $T_\parallel$ on the magnetosheath side while $T_\parallel$ again, increases significantly in the boundary layer near *D*5.

4. Summary

[50] The main results of this 3-D self-consistent global-scale hybrid simulation for cases under a steady, purely southward IMF are summarized as follows.

[51] 1. As a result of magnetic reconnection, magnetic field line configuration in the case with a 15° dipole tilt angle exhibits multiple reconnection sites around the equator and midlatitude. Flux ropes form spontaneously in between multiple X lines of finite length, which are able to generate clear bipolar signatures of the local normal magnetic field, which has been used to identify FTEs in observations. Around the noon meridian plane, contours of the B_y component show a nearly quadrupole Hall signature near FTEs due to ion kinetic effects. There usually appears an ion density enhancement of plasma core inside the flux ropes, leading to a filamentary density structure along the reconnected flux tube. Heating and multiple beams of magnetosheath ions are found inside FTEs.

[52] 2. Four types of topologies of reconnected magnetic field lines (magnetosphere-to-IMF, IMF-to-magnetosphere, IMF-to-IMF, and magnetosphere-to-magnetosphere) are obtained in the simulation, which can be explained by combinations of patchy single reconnection and multiple X line reconnection.

[53] 3. In the case in which the dipole tilt angle is 0°, single X line reconnection coexists with multiple-X-line reconnection, while the single-X-line process produces 1-D like structures. A Wałen test is performed to confirm the existence of a rotational discontinuity, which is expected for a quasi-steady like reconnection. A D-shaped ion velocity distribution with a cutoff at minimum $v_{i\parallel}$ is obtained, whereas no clear D-shaped distributions are developed in the region trailing an FTE closely.

[54] Finally, it should be noted that the scale length λ_0 used in our simulation is about 6 times larger than that in reality. The solar wind convection speed in the simulation is thus 6 times faster than the typical value in reality due to the larger Alfvén speed used in the simulation. The larger convection speed is expected to lead to a faster magnetic flux removal and a shorter reoccurrence period of FTEs at the magnetopause. In the simulation, the average time of reoccurrence of FTEs at the subsolar region is found to be $\sim 60\Omega_0^{-1}$, where $\Omega_0^{-1} \sim 1$ s is the ion gyroperiod in the solar wind. Considering the 6 times difference of the convective from reality, the recurrence period of FTEs is estimated to be 6×60 s ~ 6 min, which is comparable to that inferred from magnetosphere observations.

[55] **Acknowledgments.** This work was supported by NSF grants ATM-0646442 and ATM-0852682 to Auburn University. Computer resources were provided by the Arctic Region Supercomputer Center.

[56] Masaki Fujimoto thanks Stefan Eriksson and another reviewer for their assistance in evaluating this manuscript.

References

Birn, J., and M. Hesse (2001), Geospace Environment Modeling (GEM) magnetic reconnection challenge: Resistive tearing, anisotropic pressure and Hall effects, *J. Geophys. Res.*, *106*(A3), 3737–3750.

Birn, J., J. E. Borovsky, and M. Hesse (2008), Properties of asymmetric magnetic reconnection, *Phys. Plasmas*, *15*(3), 032101, doi:10.1063/1.2888491.

Cowley, S. W. H. (1982), The causes of convection in the Earth's magnetosphere: A review of developments during the IMS, *Rev. Geophys.*, *20*(3), 531–565.

Dorelli, J. C., and A. Bhattacharjee (2009), On the generation and topology of flux transfer events, *J. Geophys. Res.*, *114*, A06213, doi:10.1029/2008JA013410.

Dungey, J. W. (1961), Interplanetary magnetic field and auroral zones, *Phys. Rev. Lett.*, *6*(2), 47–48.

Fedder, J. A., S. P. Slinker, J. G. Lyon, and C. T. Russell (2002), Flux transfer events in global numerical simulations of the magnetosphere, *J. Geophys. Res.*, *107*(A5), 1048, doi:10.1029/2001JA000025.

Fuselier, S. A., D. M. Klumpar, and E. G. Shelley (1991), Ion reflection and transmission during reconnection at the Earth's subsolar magnetopause, *Geophys. Res. Lett.*, *18*(2), 139–142.

Gosling, J. T., J. R. Asbridge, S. J. Bame, W. C. Feldman, G. Paschmann, N. Sckopke, and C. T. Russell (1982), Evidence for quasi-stationary reconnection at the dayside magnetopause, *J. Geophys. Res.*, *87*(A4), 2147–2158.

Hasegawa, H., B. U. O. Sonnerup, C. J. Owen, B. Klecker, G. Paschmann, A. Balogh, and H. Reme (2006), The structure of flux transfer events recovered from cluster data, *Ann. Geophys.*, *24*(2), 603–618.

Kan, J. R. (1988), A theory of patchy and intermittent reconnections for magnetospheric flux-transfer events, *J. Geophys. Res.*, *93*(A6), 5613–5623.

Karimabadi, H., D. Krauss-Varban, N. Omidi, and H. X. Vu (1999), Magnetic structure of the reconnection layer and core field generation in plasmoids, *J. Geophys. Res.*, *104*(A6), 12,313–12,326.

Klumpar, D. M., S. A. Fuselier, and E. G. Shelley (1990), Ion composition measurements within magnetospheric flux-transfer events, *Geophys. Res. Lett.*, *17*(13), 2305–2308.

Kuznetsova, M. M., D. G. Sibeck, M. Hesse, Y. Wang, L. Rastaetter, G. Toth, and A. Ridley (2009), Cavities of weak magnetic field strength in the wake of FTEs: Results from global magnetospheric MHD simulations, *Geophys. Res. Lett.*, *36*, L10104, doi:10.1029/2009GL037489.

Lee, L. C., and Z. F. Fu (1985), A theory of magnetic-flux transfer at the Earth's magnetopause, *Geophys. Res. Lett.*, *12*(2), 105–108.

Lee, L. C., Z. W. Ma, Z. F. Fu, and A. Otto (1993), Topology of magnetic-flux ropes and formation of fossil flux-transfer events and boundary-layer plasmas, *J. Geophys. Res.*, *98*(A3), 3943–3951.

Lin, Y. (2001), Global hybrid simulation of the dayside reconnection layer and associated field-aligned currents, *J. Geophys. Res.*, *106*(A11), 25,451–25,465.

Lin, Y., and L. C. Lee (1994), Structure of reconnection layers in the magnetosphere, *Space Sci. Rev.*, *65*(1–2), 59–179.

Lin, Y., and X. Y. Wang (2005), Three-dimensional global hybrid simulation of dayside dynamics associated with the quasi-parallel bow shock, *J. Geophys. Res.*, *110*(A12), A12216, doi:10.1029/2005JA011243.

Lui, A. T. Y., D. G. Sibeck, T. Phan, J. P. McFadden, V. Angelopoulos, and K. H. Glassmeier (2008), Reconstruction of a flux transfer event based on observations from five THEMIS satellites, *J. Geophys. Res.*, *113*, A00C01, doi:10.1029/2008JA013189.

Omidi, N., and D. G. Sibeck (2007), Flux transfer events in the cusp, *Geophys. Res. Lett.*, *34*(4), L04106, doi:10.1029/2006GL028698.

Paschmann, G., I. Papamastorakis, W. Baumjohann, N. Sckopke, C. W. Carlson, B. U. O. Sonnerup, and H. Luhr (1986), The magnetopause for large magnetic shear: AMPTE/IRM observations, *J. Geophys. Res.*, *91*(A10), 11,099–11,115.

Phan, T. D., G. Paschmann, W. Baumjohann, N. Sckopke, and H. Luhr (1994), The magnetosheath region adjacent to the dayside magnetopause: AMPTE/IRM observations, *J. Geophys. Res.*, *99*(A1), 121–141.

Phan, T. D., G. Paschmann, and B. U. O. Sonnerup (1996), Low-latitude dayside magnetopause and boundary layer for high magnetic shear: 2. Occurrence of magnetic reconnection, *J. Geophys. Res.*, *101*(A4), 7817–7828.

Pinnock, M., A. S. Rodger, J. R. Dudeney, F. Rich, and K. B. Baker (1995), High spatial and temporal resolution observations of the ionospheric cusp, *Ann. Geophys.*, *13*(9), 919–925.

Priest, E. R., and T. Forbes (2000), Definition of reconnection, in *Magnetic Reconnection: MHD Theory and Applications*, 231–245 pp., Cambridge Univ. Press, Cambridge, U. K.

Pritchett, P. L. (2001), Geospace environment modeling magnetic reconnection challenge: Simulations with a full particle electromagnetic code, *J. Geophys. Res.*, *106*(A3), 3783–3798.

Raeder, J. (2006), Flux transfer events: 1. Generation mechanism for strong southward IMF, *Ann. Geophys.*, *24*(1), 381–392.

Rijnbeek, R. P., S. W. H. Cowley, D. J. Southwood, and C. T. Russell (1984), A survey of dayside flux transfer events observed by Isee 1 and 2 magnetometers, *J. Geophys. Res.*, *89*(A2), 786–800.

Russell, C. T., and R. C. Elphic (1978), Initial ISEE magnetometer results: Magnetopause observations, *Space Sci. Rev.*, *22*(6), 681–715.

Scholer, M. (1988), Magnetic-flux transfer at the magnetopause based on single X line bursty reconnection, *Geophys. Res. Lett.*, *15*(4), 291–294.

Scholer, M., I. Sidorenko, C. H. Jaroschek, R. A. Treumann, and A. Zeiler (2003), Onset of collisionless magnetic reconnection in thin current sheets: Three-dimensional particle simulations, *Phys. Plasmas*, *10*(9), 3521–3527, doi:10.1063/1.1597494.

Scudder, J. D., P. A. Puhl-Quinn, F. S. Mozer, K. W. Ogilvie, and C. T. Russell (1999), Generalized Walén tests through Alfvén waves and rotational discontinuities using electron flow velocities, *J. Geophys. Res.*, *104*(A9), 19,817–19,833.

Shay, M. A., J. F. Drake, B. N. Rogers, and R. E. Denton (2001), Alfvenic collisionless magnetic reconnection and the hall term, *J. Geophys. Res.*, *106*(A3), 3759–3772.

Sibeck, D. G., and R.-Q. Lin (2010), Concerning the motion of flux transfer events generated by component reconnection across the dayside magnetopause, *J. Geophys. Res.*, *115*, A04209, doi:10.1029/2009JA014677.

Sonnerup, B. U. Ö. (1979), Magnetic field reconnection, in *Solar System Plasma Physics*, edited by L. T. Lanzerotti, C. F. Kennel, and E. N. Parker, pp. 45–108, North-Holland, New York.

Sonnerup, B. U. Ö., and L. J. Cahill Jr. (1967), Magnetopause structure and attitude from Explorer 12 observations, *J. Geophys. Res.*, *72*(1), 171–183.

Sonnerup, B. U. Ö., G. Paschmann, I. Papamastorakis, N. Sckopke, G. Haerendel, S. J. Bame, J. R. Asbridge, J. T. Gosling, and C. T. Russell (1981), Evidence for magnetic-field reconnection at the Earth's magnetopause, *J. Geophys. Res.*, *86*(A12), 10,049–10,067.

Swift, D. W. (1996), Use of a hybrid code for global-scale plasma simulation, *J. Comput. Phys.*, *126*(1), 109–121.

Terasawa, T. (1983), Hall current effect on tearing mode instability, *Geophys. Res. Lett.*, *10*(6), 475–478.

Winglee, R. M., E. Harnett, A. Stickle, and J. Porter (2008), Multiscale/multifluid simulations of flux ropes at the magnetopause within a global magnetospheric model, *J. Geophys. Res.*, *113*(A2), A02209, doi:10.1029/2007JA012653.

Wu, B. H., and L. C. Lee (2000), Hall effects on the Walén relation in rotational discontinuities and Alfvén waves, *J. Geophys. Res.*, *105*(A8), 18,377–18,389.

Y. Lin, J. D. Perez, B. Tan, and X. Y. Wang, Physics Department, Auburn University, 206 Allison Lab., Auburn, AL 36849-5311, USA. (ylin@physics.auburn.edu; perez@physics.auburn.edu; tanbiny@auburn.edu; xywang@physics.auburn.edu)